Combustion and Flame 234 (2021) 111724

Contents lists available at ScienceDirect

Combustion and Flame

journal homepage: www.elsevier.com/locate/combustflame

Analysis of the wind flow and fire spread dynamics over a sloped–ridgeline hill

Abdelrahman Abouali*, Domingos Xavier Viegas, Jorge Rafael Raposo

ADAI/CEIF (Forest Fires Research Center), University of Coimbra, Rua Luis Reis dos, Santos, Coimbra 3030-788, Portugal

ARTICLE INFO

Article history:
Received 14 March 2020
Revised 29 August 2021
Accepted 29 August 2021

Keywords:
Fire channelling
Lateral fire spread
Sloped–ridgeline hill
Fire-induced wind
Fire–terrain–wind interactions

ABSTRACT

This paper presents results from a computational and laboratory investigation of wind flow and fire spread over an isolated sloped-ridgeline laboratory-scale hill under various slopes with the wind blowing perpendicularly to the ridgeline. The results show two situations of unexpected or unusual fire behaviour; one is a lateral spread of the fire front over the windward face into a down-ridge direction resulting from a strong near-surface flow component parallel to the ridgeline. The other behaviour is a lateral enlargement of the fire front near the ridgeline over the leeward face in an up-ridge direction resulting from a flow parallel to the ridgeline. Comparison with reference fire spread rates and wind flow observations highlight the importance of the interaction between terrain-modified flow mechanisms and the fire in which they result in accelerated flows that drive the indicated unexpected behaviour.

1. Introduction

The wind, topography and fuels are widely recognised as the dominant factors affecting forest fire behaviour in which their mutual multi-scaled physical interactions may result in unexpected fire behaviour [1–4]. The fire spread over complex topography is a very common field situation in which these interactions are important, and the resultant dynamic fire growth is a challenge in terms of prediction and hazard management.

Current operational fire spread prediction models, which [5–7] summarise some of them, typically assume that the rate of spread will remain constant unless there is a change in the underlying fire environment conditions. This steady-state assumption can be invalid for dynamic modes of fire spread, in which the rate of spread can vary greatly due to interactions between the fire and the surrounding environment. Understanding the physical processes that trigger these dynamic modes of fire spread is, therefore, a key step towards improving the planning of wildfire management operations.

It is well known that terrain slope has a significant effect on the fire spread, as generally, the fire spreads with higher rate of spread in up-slope directions and with slower rate of spread over down-slopes with steady state behaviour. Also, on the presence of a favourable wind, the fire's rate of spread will be increased. However, in the presence of both wind and slope, the behaviour depends on the magnitude of both effects and the behaviour of the fire is usually dynamic [8].

Several numerical and experimental studies were carried out to analyse the fire behaviour over complex topography namely on slopes and hills [8–14]. However, we still lack understanding about fire spread in complex topography and the interactions between wind flow, topography, and fire dynamics. In this paper, we are concerned with the fire behaviour associated with the interaction between terrain-modified winds over a sloped-ridgeline hill and fire-induced convection (flow).

Previous studies [9,15] showed that, for a fire spreading over the leeward face of a hill with the wind blowing perpendicularly to the hill's ridgeline, a lateral enlargement of the fire front near the ridgeline occurs. McRae [15] who first noticed this phenomenon designated it as 'fire channelling' or 'lee-slope channelling'. Sharples [9] have investigated the phenomena based on real-fire observations, where analysis of several possible mechanisms revealed that hill's lee-slope eddy plays a crucial role in driving the fire channelling process. Simpson [10] has shown through large-eddy simulations that the lateral fire enlargement is driven by an updraft–downdraft interface movement across the fire perimeter. The inflow and outflow associated with these updrafts and downdrafts resulted in either clockwise or counter-clockwise flow rotation at the mid-flame height near the flanks of the fire. He proposed that the process is a result of an

* Corresponding author.
E-mail address: awabuali@hotmail.com (A. Abouali).

https://doi.org/10.1016/j.combustflame.2021.111724

interaction between the fire-induced convection (pyro-convection) and the terrain-modified winds through mechanisms that still need to be investigated. An experimental study by Raposo [11] conducted on a two-dimensional hill (horizontal ridgeline) with a perpendicular flow relative to the ridgeline showed that the fire enlarges symmetrically towards the two lateral directions near the top of the crest due to the interaction between fire and wind.

In the present paper, we analyse the fire behaviour over a sloped-ridgeline hill, which is a typical configuration in nature as can be seen for example at the end of a ridge which height is gradually reduced. During fire propagation preliminary tests over a laboratory-scale configuration, we noticed a lateral non-symmetric fire growth behaviour over the hill's leeward face. This behaviour is similar to the earlier mentioned fire channelling phenomena, but in this case, it is not symmetric. We also noticed another fast and non-symmetric lateral growth behaviour over the windward face of the hill. It is important to investigate these two non-symmetric fire growth behaviours as the nature of the configuration where the fire's driving conditions, namely terrain-modified wind and slope, are changing along the ridgeline. The investigation of the sloped-ridgeline hill being a generalization of the previous case contributes to a better understanding of the fire enlargement phenomena (fire channelling) over hills. The investigation is made by performing a set of laboratory-scale experiments for a fire spreading over a physical model, complemented by physical and numerical analysis of the adiabatic flow around a similar hill.

To our knowledge this investigation involves for the first time a careful analysis of the adiabatic flow around a sloped-ridgeline hill under various wind and slope conditions using computational fluid dynamics (CFD) simulations validated by experimental measurements in a wind tunnel. The analysis of the terrain-modified flow is used to interpret the results obtained in a set of laboratory-scale experiments of fire spread.

2. Methods and materials

2.1. Hill configuration and terminology

The shape of the sloped-ridgeline hill is shown schematically in Fig. 1. The two faces of the hill are identical and have the shape of a right-angled triangle. To minimise the effect of the Reynolds number on the location of flow separation, we adopted a sharp ridgeline. The angle between each face and the horizontal reference is α resulting in a symmetrical triangular cross-section hill.

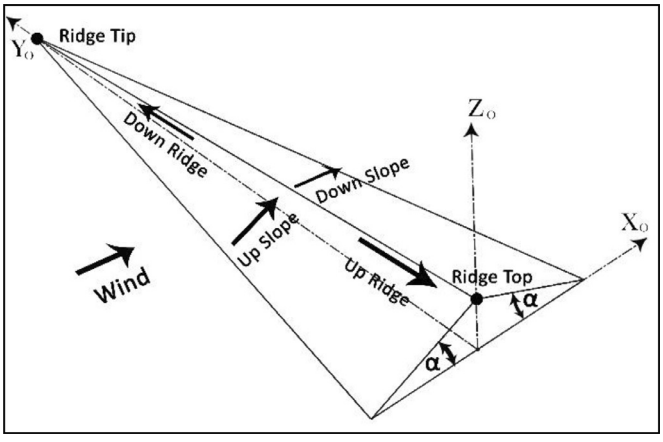

Fig. 1. Schematic view of the 3D hill with the terminology used for the main flow/fire spread directions.

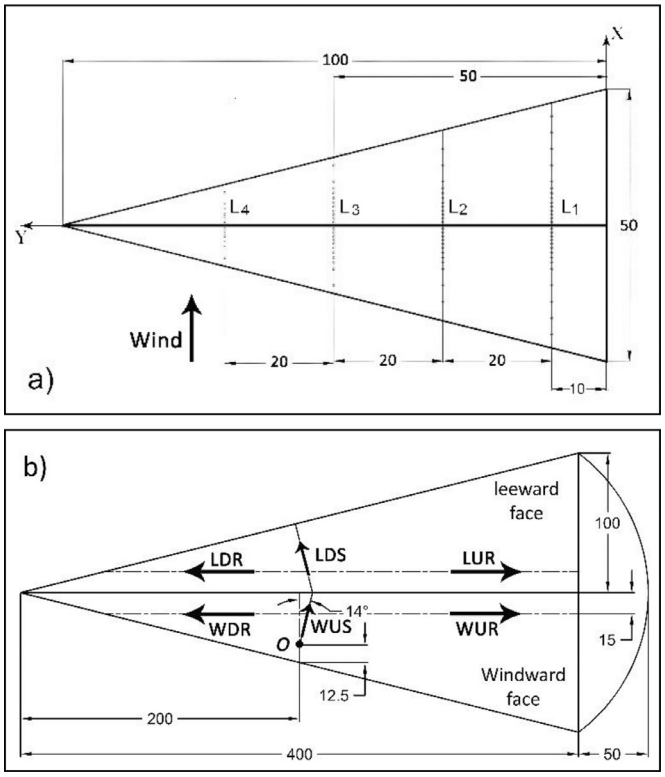

Fig. 2. a) Plan view of the model used in the wind tunnel tests. The location of the four lines where we distributed the pressure taps are shown. The dimensions are indicated in cm. b) Plan view of the model used in the Combustion Tunnel tests and the six directions used to evaluate the ROS of the fire are shown. The ignition occurs at the point labelled by O. The dimensions are indicated in cm.

2.2. Model's scale and dimensions

We use similar models for the adiabatic flow and the fire experiments, but with different dimensions. We used a return type wind tunnel for the adiabatic flow investigation and non-return combustion tunnel for the fire investigation. For the fire experiments, the triangular face of the model was 4 m long and 1 m wide. Due to the limitation on the wind tunnel's working section the size of the model was reduced four times for the adiabatic flow experiments and CFD simulations (Fig. 2a, b). However, to keep Reynold's number based on the hill's height within the same order of magnitude ($\sim 10^5$), we increased the flow velocity four times in the smaller scale experiments and simulation.

We are aware that the fire experiments at laboratory scale do not fulfil all the scaling requirements, as for example the equality of the relative dimensions of hill height and flame length or Froude number, but the effect of these discrepancies on the features of the observed fire spread phenomena must be relatively small in comparison to the changes produced on the flow by the modification of the geometry of the hill. In previous studies that are related to canyons and 2D hills [11,16,17], the authors observed that using this partial similarity simulation with relatively small physical models it is possible to obtain relevant features of fires in complex terrain and flow configurations with practical relevance.

2.3. Adiabatic flow experiments setup

Experimental analysis of the flow around an isolated sloped-ridgeline hill was performed in the wind tunnel of the Industrial Aerodynamics Laboratory (LAI) of University of Coimbra. The wind tunnel is of return type with an open test section of 5 m length by 2 m width and 2 m height, with a maximum velocity of 20 m s^{-1}.

We used a model made of wood with a smooth surface with the dimensions shown in Fig. 2a. The model was fixed to the floor of the tunnel's working section where its ridgeline is at 2.5 m from the wind inlet and centred between the two lateral edges of the working section. The ridgeline was perpendicular to the flow direction. Three values of slope inclination angles α were used: 25, 35 and 45º (cf. Fig. 1). To minimise the end effects of the model, we added a triangular plate at the end of the model to close the gap between the two slopes.

Static pressure taps were placed along four lines in each face of the hill's model, as shown in Fig. 2a. The 1st line has 28 taps and 45 cm length, the 2nd line has 24 taps and 35 cm, the 3rd line has 22 taps and 25 cm, and the 4th line has 12 taps and 15 cm length making a total of 86 pressure taps on both faces. The pressure taps along each line are spaced at smaller distances (~1 cm) near the ridgeline and at larger distances (~3 cm) near the base (Fig. 2a).

We identify each pressure tap by its distance x_{ij} in the plane form, measured along the i order line from the base edge of the windward face to the pressure tap. In order to simplify the presentation of the results, we will use the non-dimensional coordinate x'_{ij} defined by Eq. (1).

$$x'_{ij} = x_{ij}/L_i \tag{1}$$

Where L_i is the length of the line of order i, which is 45, 35, 25 and 15 cm respectively from the first line to the last; x'_{ij}=0.5 corresponds to the ridgeline in all cases.

The flow in the tunnel is produced in neutral atmospheric conditions. The free stream velocity is measured by a pitot tube fixed at the centre of the flow entrance of the working section (1 m from the ground). Flow is adjusted to achieve a free stream velocity of 8 m s^{-1}. For the analysis, the pressure is measured using a Multur digital pressure gauge model EMA 84, which has a margin of error of ± 0.2%. Then we calculated the pressure coefficient (C_p) at the 86 taps using Eq. (2).

$$C_p = \frac{p - p_\infty}{1/2\ \rho_\infty\ U_\infty{}^2} \tag{2}$$

Where $p - p_\infty$ is the difference between the static pressure measured at the tap and the freestream pressure; ρ_∞ is the density of the freestream air which is taken by 1.2 kg/m^3 constant for all the tests; U_∞ is the velocity of the freestream, measured using the pitot tube.

For flow visualisation, we used wool tufts to evaluate the flow topology. The tufts have a length of ~5 cm and were placed randomly to cover the face area, but with the consideration that they are spaced between each other with a distance larger than their lengths to minimize interference.

2.4. CFD simulation setup

We performed a CFD simulation of the flow around the sloped-ridgeline hill using the open-source CFD software OpenFOAM-4.1 [18]. The dimensions of the simulation domain consist of a box with dimensions 2.5 m length (x-direction), 2.0 m width (y-direction) and 1.5 m height (z-direction) (Fig. 3). The hill was placed at a distance of 0.8 m between the inlet section and the model's first point (corner) reached by the wind (Fig. 3a).

The flow is assumed incompressible and adiabatic. The inlet flow is steady with a uniform velocity of 8.0 m s^{-1}. It is assumed that there is no flow across the lateral and the top boundaries of the domain (wall type boundaries). The flow near the ground is a boundary layer type developed upwind of the hill. Initially, the pressure is considered uniform and equal to 1 atmosphere in all the domain.

The mesh was created using OpenFOAM's tool SnappyHexMesh [19]. We created a coarse structured mesh with a cell size of 0.05 m then refined and snapped the mesh to the hill. The refinement is characterised by its level where level 0 corresponds to the coarsest mesh (0.05 m), and then each refinement level has a cell size equal to half the size of the previous level (i.e. level 1 will has a cell size of 0.025 m). We divided the domain into three regions A, B and C (Fig. 3) which have different levels of refinement. Region A coincides with the calculation domain and regions B and C are surrounding the model. Their heights (z-direction) equal to 3.45 and 1.15 times the height of the model, respectively. Their widths (y-direction) are 1.4 and 1.2 times the width of the model respectively, where the regions are centred with the model in the y-direction. Their limits start at 0.2 m and 0.1 m along the x-direction measured from the farthest corner of the windward face and end at 8 and 4 times the height of the model respectively measured from the farthest corner of the leeward face. The three regions have refinement levels of 1, 3 and 4, respectively. The mesh then snapped to the model with accuracy of 7 to 9 refinement level depending on the refinement needed for the snapping. On all the transitions between a refinement level and another, we added four transition cells to assure a smooth level transition

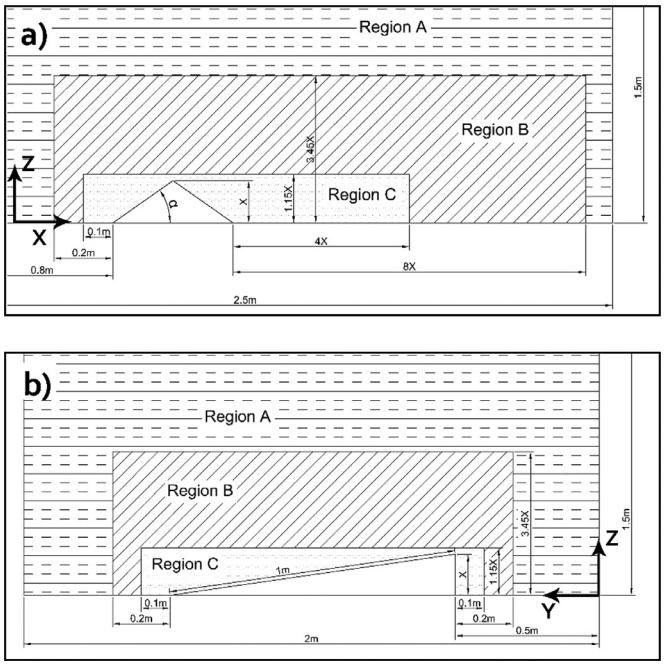

Fig. 3. Two cross-sections on the calculation domain showing the axes directions, refinement regions with their dimensions and the position of the model a) parallel to the wind direction. b) Perpendicular to the wind direction.

We tested several meshes, turbulence model algorithms and OpenFOAM solvers. The present results were obtained from Reynolds-averaged Navier–Stokes equations (RANS) simulation using the SimpleFoam Solver with the k-ω Shear Stress Transport (SST) turbulence model [20] and the SIMPLEC algorithm for the pressure equation. We selected these models and the mesh based on a convergence study, where the convergence was tested against the obtained pressure results from the adiabatic wind tunnel experiments. The reported results achieved convergence criteria composed of two factors to be satisfied. The first factor is a mean squared error less than 15% on the pressure measurements at the indicated 86 pressure tap locations on the wind tunnel tests (Fig. 2a). The second factor is a residual error on the CFD solution less than 5E-4.

We simulated the flow for the same three cases tested experimentally in the wind tunnel (α = 25, 35 and 45º) plus two other cases (α = 20 and 10º) that were used in our fire spread

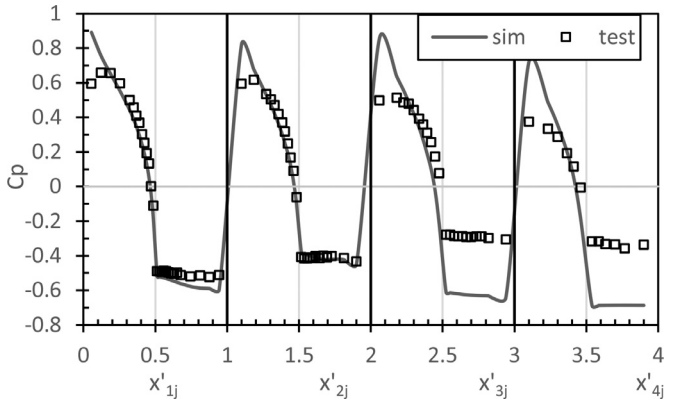

Fig. 4. A comparison between the wind tunnel measurements and the CFD simulation results for the wall pressure coefficient values in the case of α=45° Each unit of the x-axis represents one of the four lines, where the first line is plotted from $x=0$ to 1 and the second line is from $x=1$ to 2 and so on. The vertical grey lines (at $x=0.5$, 1.5, ...) represent the ridgeline.

Fig. 5. Image showing the hill model placed in the combustion wind tunnel during one of the experiments, the rounded end is attached to the left side of the model.

experiments, to support the interpretation of the flow topology in varying geometry and reference flow conditions. A comparison between the pressure results of the simulation and the measurements of the wind tunnel is presented in Fig. 4 for $\alpha = 45^{o}$. We can notice that the numerical solution did not predict well the flow at the base of the windward face and the down-ridge half of the leeward face. Otherwise, the solution is reasonably accurate. The same agreement and disagreement areas on the solution are noticeable for the other two cases. We find that refining the solution more on these areas would not be cost-effective since our study is not mainly focused on the CFD simulation. Furthermore, in spite of these discrepancies, we consider that combining the observations from both adiabatic wind tunnel experiments, and the numerical solution is enough to assist in interpreting the fire behaviour, as we shall see later.

2.5. Fire spread experiments setup

In these experiments, we consider a sloped-ridgeline hill of the same geometry that we described above, covered by fuel and subjected to a surface fire that is originated from a single point on the windward face of the hill, spreading as a flaming fire front along the hill. We, therefore, exclude spot and crown fires that may occur in a real fire.

The physical model has the dimensions shown in Fig. 2b and is composed by two triangular steel plates covered by a metallic grid to hold the fuel bed particles. The used α values in the fire experiments were 10, 20, 25, 35 and 45º (cf. Fig. 1). The hill model was placed at the centre of the Combustion Wind Tunnel of the Forest Fire Research Laboratory of the University of Coimbra, in Lousã (Portugal), where its ridgeline is at a distance of 4 m from the wind inlet. The combustion tunnel has an open working area of 6×8 m^2 with two lateral 2 m high walls but without ceiling (Fig. 5). To our knowledge this is the largest combustion wind tunnel that is used for wildfire tests. The flow is generated by two axial fans of 72 kW that can produce a flow with a maximum reference velocity of 7 m s^{-1}. The rotational speed of the fans controls the flow velocity. Great care was taken to assure that the flow in the Combustion Tunnel is uniform across the test section (perpendicular to the flow). The flow over the floor of the tunnel is of a boundary layer type with a reference velocity U_o that is measured at the centre of the working section floor and 0.5 m above the ground in the absence of the model. The fire experiments were performed with the following values of U_o: 0, 1, 2 and 3 m s^{-1} for each inclination value of the slope.

A rounded body was built for each value of α and attached to the model at its open end (up-ridge) to produce a smooth flow around the hill, as shown in Fig. 5. This procedure was taken to reduce the end effects on the propagation of the fire. The distance between the model and the lateral walls of the tunnel was ~0.8 m on both sides.

A uniform fuel bed composed of dead pine needles (*Pinus Pinaster*) with a load of 0.6 kg m^{-2} (dry basis) and an average depth of 0.05±0.01 m covered the two faces of the model. The used fuel has an average surface area to volume ratio (SAV) of ~ 2640 m^{-1}. The fuel moisture content was measured for each set of experiments with an A&D ML50 moisture analyser, and the amount of moisture was compensated to keep the fuel-loading constant based on a dry basis. The range of values of the moisture content in the tests was 8.9%<m_f<13.3% (dry basis). We define the set of tests as a group of experiments performed on the same day while the change in moisture content does not exceed ±0.5% during the whole testing period.

For each set of tests, we define a basic rate of spread (ROS) Ro that is determined by performing a reference test in no-wind and no-slope conditions. We used a flat 1m2 table with strings taut over the fuel bed and spaced 10 cm between them to perform the reference test. The time taken by the fire to pass from a string to another was measured. The basic ROS is defined as the slope of the linear fitting between the time versus distance, following [3]. The parameters of the performed tests and designations are reported in Table 1. To avoid ambiguity in the tests reference we use the following designation form: [3D (test#).(Uo).(α)].

The fire was ignited at an origin point O on the middle of windward face 0.125 m above the base of the hill that corresponds to 25% of the face width at that mid-section (Fig. 2b). The airflow was then turned on to a pre-adjusted velocity. An IR camera, a video camera and several digital cameras were used to record the fire spreading over the hill. The obtained images (frames) from the IR recording were analysed using the open-source software Fire ROS Calculator [21], which calibrates the camera and determine the ROS values along user-defined directions. It was found that the error margin of the Fire ROS Calculator outputs is of ± 5% [21]. Besides, for flow visualization, we used a 3000 W pointer laser that is diverged into a laser sheet using a plane-concave cylindrical lens with a focal length of 25 mm. We added a remotely controlled smoke generator in the middle of the combustion wind tunnel at the wind entrance and near the ground to assist in visualizing the flow.

Table 1
Average ROS of the fire on the predefined six directions for each test along with their confidence intervals.

Test ref.	α (°)	U (m/s)	Ro (cm/s)	R'_{WUS}	R'_{LDS}	R'_{WUR}	R'_{LUR}	R'_{WDR}	R'_{LDR}
3D29.0.10	10	0	0.30	0.68± 6%	0.65± 18%	1.03± 44%	1.02± 44%	0.6 1± 12%	0.72± 0%
3D30.1.10	10	1	0.30	3.13± 2%	1.77± 18%	0.74± 14%	0.78± 4%	0.65± 4%	0.78± 4%
3D31.2.10	10	2	0.30	7.57± 8%	1.58± 14%	0.71± 18%	1.15± 2%	0.72± 12%	1.18± 6%
3D32.3.10	10	3	0.31	10.21± 2%	2.47± 0%	0.83 E	2.63± 20%	0.73 E	1.51± 12%
3D25.0.20	20	0	0.30	1.07± 4%	0.54± 4%	1.13± 12%	1.13± 10%	0.84± 10%	1.01± 32%
3D26.1.20	20	1	0.28	2.24± 0%	1.15± 4%	0.82± 4%	2.19± 2%	0.71± 18%	1.03± 2%
3D27.2.20	20	2	0.28	5.31± 8%	1.06± 2%	0.91± 20%	3.63± 16%	0.63± 10%	1.25± 0%
3D28.3.20	20	3	0.28	8.13± 14%	1.10± 20%	1.39± 32%	5.86± 2%	1.01± 6%	2.20± 22%
3D1.0.25	25	0	0.28	1.16± 14%	0.60± 12%	0.79± 14%	0.93± 6%	0.68± 20%	0.73± 34%
3D2.1.25	25	1	0.28	4.37± 2%	0.70± 24%	0.37 E	2.81± 12%	0.83 E	1.12± 18%
3D3.2.25	25	2	0.29	6.24± 16%	0.95± 2%	0.92 E	4.07± 0%	0.66 E	1.15± 0%
3D4.3.25	25	3	0.29	6.25± 0%	1.07± 24%	0.83 E	5.52± 12%	0.48 E	2.24± 2%
3D5.0.35	35	0	0.31	1.72± 24%	0.80± 30%	0.73± 34%	0.94± 26%	0.66± 4%	0.81± 18%
3D6.1.35	35	1	0.30	4.59± 2%	0.89± 0%	0.84± 38%	1.19± 12%	1.17± 4%	3.09± 0%
3D7.2.35	35	2	0.30	6.86± 0%	1.14± 8%	0.93 E	1.45± 10%	1.18± 14%	4.11± 8%
3D8.3.35	35	3	0.30	9.94± 8%	1.14± 6%	1.98 E	5.21± 2%	3.28± 6%	3.89± 6%
3D9.0.45	45	0	0.28	1.34± 20%	0.94± 12%	0.86± 6%	0.90± 12%	0.79± 2%	1.01± 0%
3D10.1.45	45	1	0.28	4.46± 0%	1.00± 22%	0.81± 6%	3.02± 20%	2.02± 10%	2.18± 6%
3D11.2.45	45	2	0.26	6.00± 0%	0.97± 14%	0.51 E	3.08± 8%	2.87± 8%	2.86± 4%
3D12.3.45	45	3	0.28	3.69± 8%	1.65± 12%	1.21 E	5.95± 20%	4.61± 0%	3.66± 8%

E: self-extinguished fire, which is the case where the fire self-extinguished after spreading a small distance, however the presented ROS value is for that small distance. The test references have the designation: (3D)(Test #).(Uo).(angle).

2.6. Fire spread analysis methodology

Using the above procedure, we obtain the fire contours or isochrones evolution at given time steps for each test. To better interpret the properties of the fire spread, we define the following directions to estimate the ROS along them (Fig. 2b):

- WUS – Upslope over the windward face. This direction is along a line that has an angle of 14° relatively to a perpendicular to the ridgeline originated from the ignition point *O* and towards up-ridge. We choose this angle since the maximum rate of height change (i.e. the maximum slope) direction at the ignition point has an inclination close to that value.
- LDS –Downslopeover theleewardface. Along a line that has an angle of 14° relatively to a perpendicular to the ridgeline originated from the intersection of the WUS line with the ridgeline and towards down-ridge.
- WUR – Up-ridge over the windward face. This direction is parallel to the ridgeline at an average distance of 0.15 m from it. It starts from the middle of the ridgeline and ends at the up-ridge end.
- LUR – Up-ridge over theleewardface. The direction has the same remarks as on the WUR. However, in some cases, the ROS was measured along a line that is connecting the most advanced point of the fire front on the up-ridge direction regardless of its distance from the ridgeline but always parallel to it.
- WDR – Down-ridge over the windward face. This direction is collinear with the up-ridge direction line, but it starts from the middle of the ridgeline and ends at the down-ridge end.
- LDR – Down-ridge over theleewardface. This direction has the same remarks as for WDR.

Considering two positions, P_i and P_{i+1}, of the fire front along a given direction detected at time t_i and t_{i+1}, and distances d_i and d_{i+1} measured from the same reference, we can determine the instantaneous value of the ROS as:

$$R(t) = (d_{i+1} - d_i)/(t_{i+1} - t_i) \tag{3}$$

Assuming that the fire spread along the reference direction is steady, knowing the distances d_k of the fire front position at a set of times t_k ($k = 1 \ldots n$), we can determine the average ROS ($\bar{R}$) of the fire along that direction by calculating the slope of the linear fitting between the two data sets [22]. In our analysis, we considered a time-lapse not less than 5 s or greater than 30 s to calculate the average ROS, which produced four data points in minimum for each direction.

Although in the general case the fire spread is not steady according to [3], we shall consider average values of the ROS along the six above mentioned directions like for example $\bar{R}_{WUR}$ and $\bar{R}_{LUR}$. Furthermore, for each direction we calculate the average ROS along several close and parallel lines, which can better characterize the average ROS ($\bar{R}$) of the fire in an indicated direction to minimize local effects.

To ensure the reliability of the results, we replicated the experiments and calculated a confidence interval (CI) for the results of $\bar{R}$ in each direction. The value of CI is expressed as a percentage of the average of the values of $\bar{R}$ obtained in the replications. If the percentage was lower than 20% in all directions, we consider the results reliable. In the opposite case, we replicated the experiment until the calculated CI became less than 20% in all six directions using the values of $\bar{R}$ obtained in any two replications. However, for the ROS values that are close to R_o, the reliability condition is increased from 20% to 50%. The CI is calculated according to Eq. (4).

$$CI = NORMSINV \times \frac{1-\alpha}{2} \times \frac{\sigma}{\sqrt{n}} \tag{4}$$

Where *NORMSINV* is a Microsoft Excel (2016) iterative function that returns the inverse of the standard normal cumulative distribution. In this equation we have:

- α is taken by 0.05 for all tests.
- σ is the standard deviation based on the entire population (n).
- n is taken by two always as the *CI* is calculated between the results of two repetitions.

To minimise the effect of small variations of fuel bed properties, namely moisture content, following [23], we use the non-dimensional ROS (NDROS) (R') values given by Eq. (5).

$$R' = R/R_o \tag{5}$$

In Eq. (5), R_o is the basic ROS measured in no-slope and no-wind conditions, which we measure for each testing session.

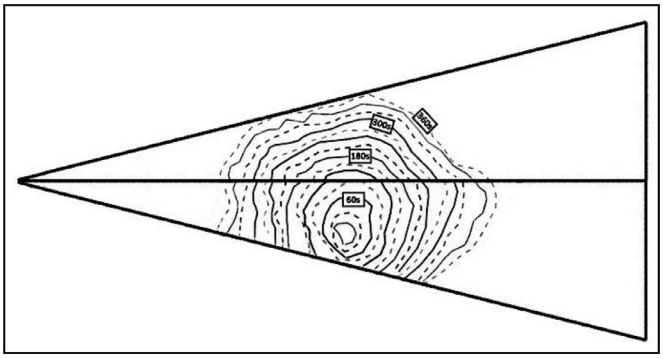

Fig. 6. Fire propagation isochrones contour map for test 3D1.0.25, with α=25° and U_o=0 m.s^{-1}. The time-lapse between frames is 30 s.

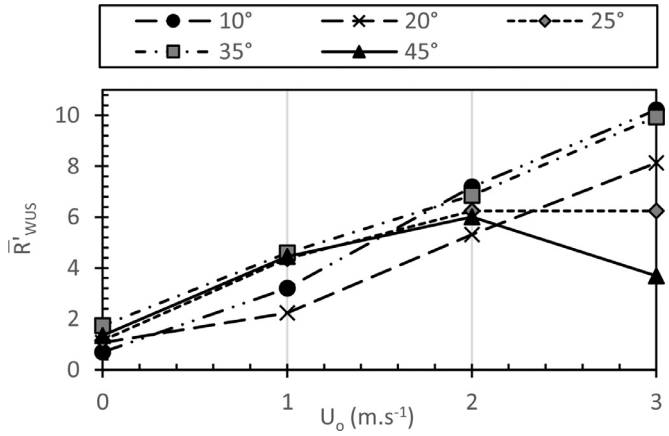

Fig. 7. The average NDROS values on the windward upslope direction (WUS).

In the overall context of fire safety, we consider that we are in the presence of an unexpected or unusual fire behaviour if *R'* reaches values greater than 5 or has a rate of change higher than 5 units.min^{-1} for a given direction, as these may correspond to intense or rapidly changing fire spread conditions that may endanger fire suppression agents.

3. Results and discussion

We discuss first the observed overall fire behaviour over the sloped-ridgeline hill configuration; then we present some results of the fire behaviour processes making use of the adiabatic flow study to analyse and interpret them.

3.1. Overall fire behaviour

Starting with the no-wind scenario, as shown in Fig. 6 for test 3D1.0.25, the fire spreads with consistent rates in all directions except for the WUS, where the slope effect takes place. The pattern

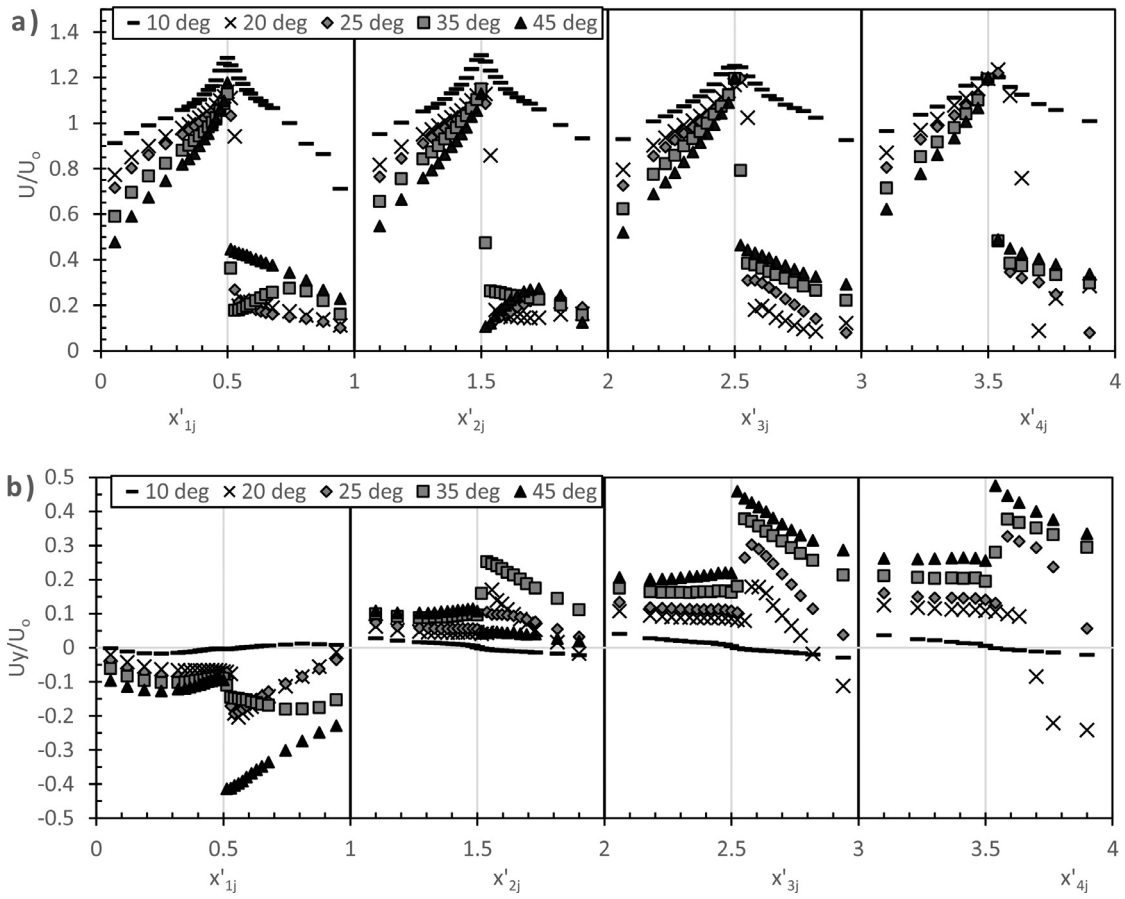

Fig. 8. Flow velocity results from the CFD simulation are presented. The values are calculated on a plane parallel to the surface of the hill and spaced 0.01 m above it. The points are distributed along the same four lines presented in Fig. 2a. The velocity is presented dimensionless where the values are divided by the inlet stream velocity (U_o = 8 m s^{-1}). Each unit on the x-axis represents the full length of each of the four lines. a) Velocity modulus. b) Velocity component in the y-direction (U_y). The vertical grey lines represent the ridgeline.

Table 2
Maximum R'_{LUR} and R'_{WDR} values and maximum rate of change of ROS with time for all the tests with wind condition.

Test Ref.	Max. R'_{LUR}	Max. rate of change ($R'_{LUR}.min^{-1}$)	Max. R'_{WDR}	Max. rate of change ($R'_{WDR}.min^{-1}$)
3D30.1.10	1.11	N/A	1.23	N/A
3D31.2.10	1.24	N/A	2.80	N/A
3D32.3.10	1.94	N/A	E	N/A
3D26.1.20	3.51	5.0	1.05	N/A
3D27.2.20	4.25	6.9	0.99	N/A
3D28.3.20	8.00	12.6	1.56	N/A
3D2.1.25	6.52	4.5	E	N/A
3D3.2.25	7.43	7.1	E	N/A
3D4.3.25	11.30	9.3	E	N/A
3D6.1.35	6.06	5.2	3.95	9.1
3D7.2.35	7.92	19.5	2.21	12.6
3D8.3.35	12.52	15.6	8.61	45.0
3D10.1.45	7.59	6.0	3.20	5.6
3D11.2.45	9.58	9.5	4.41	9.0
3D12.3.45	12.59	10.9	9.22	23.4

E: extinguished fire, on these cases the fire was self- extinguished after spreading a small distance in this specific direction.

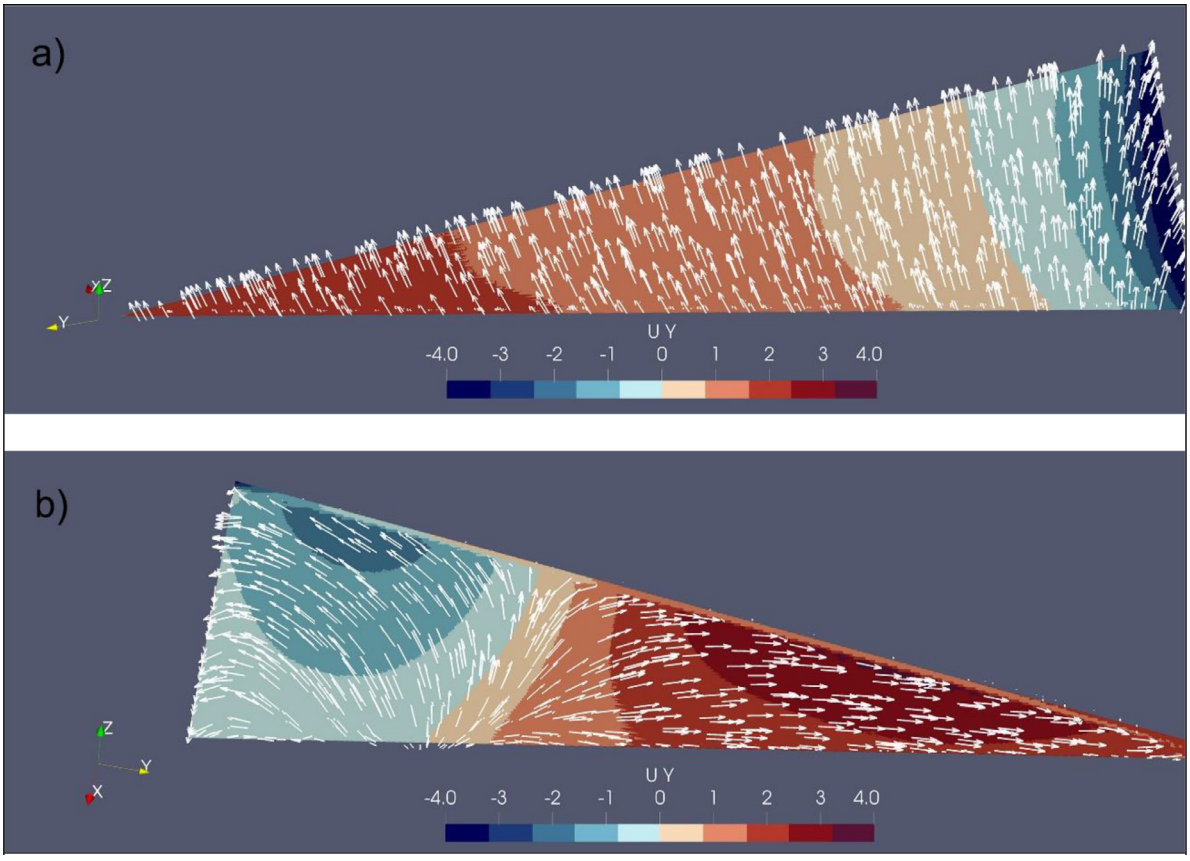

Fig. 9. Numerical results for the field of the velocity component in the y-direction (U_y) on parallel planes to the hill's faces and spaced from them by 0.01 m for α=35º along with the velocity vectors. a) The windward face. b) The leeward face.

shape of the fire contours is similar for all α values, which is a typical shape for a point-ignited fire.

When the wind flow is present, the fire starts to spread in the WUS direction with relatively higher values in comparison to the other two directions on the same face, WUR and WDR, where the fire spreads with rates close to the basic ROS value (R_0), $R' \approx 1$. However, when α>25º the value of the ROS becomes quite large due to change in the near-surface wind velocity and direction. We will detail this increase in ROS in the next subsections of the discussion.

After the fire passes the ridgeline, it spreads laterally over the leeward face near the ridgeline but without symmetry between the two directions, LUR and LDR, where the spread is more rapid in the LUR. In the LDR direction, the fire spreads slower except for α >25º, as the fire starts to enlarge in that direction as well, but not as rapidly as in the LUR. Finally, the fire spreads towards LDS direction with $R' \approx 1$.

We report the average NDROS values of the fire spread in the six directions in Table 1. The reported results are the average values of the two replicates that gave the lowest CI value for each test

configuration. The associated basic ROS (R_o) values range between 0.23 and 0.33 cm s^{-1}. The values of R_o associated with each test are reported in Table 1. Similarly, to the NDROS values, the presented R_o values are an average also of the R_o of the two replicates that are considered for each test.

On the following three subsections, we discuss in detail the fire behaviour in the six directions and their instantaneous and average ROS results. As it is not convenient to present the instantaneous ROS values averaged from the two replications, for each test we will present only the results from the last considered replication.

In Table 2, we present the maximum ROS values achieved during our tests by a fire spreading on the LUR and the WDR directions since we are focusing more on them as the fire mostly shows an unexpected behaviour on these directions. We also present on the same table the rate of change of the ROS per minute. These results indicate how intense and rapid the fire's ROS may develop in time, which is important in an operational context.

3.2. Fire spread in the up and downslope directions

Over the terrain configuration in hand, the spread on the WUS direction shows a typical behaviour where we can find that the NDROS values increase with α in the no-wind condition (Fig. 7). However, in the presence of wind, the behaviour is the opposite for most α values, where $\overline{R'}_{WUS}$ values decrease with the increase in α (i.e. the lowest obtained ROS value at the R highest wind speed is for the highest slope). This behaviour is contrary to the expected behaviour in an upslope direction.

In Fig. 8, we present the modulus of the flow velocity in the absence of fire calculated from the CFD simulation. We calculated the values along the same four lines used to calculate C_p (Fig. 2a), but on a parallel plane spaced 1 cm above the surface of the hill, for values of α=20, 25, 35 and 45º. We can notice that the velocity modulus of the flow near the windward face is higher for lower values of α (Fig 8a). In addition, the flow reaches a maximum velocity near the ridgeline, and its value does not depend much on α. This result matches the measurements taken from the wind tunnel tests in the absence of fire. Furthermore, due to the nature of the slope, we can notice that with increasing α, an increase in the U_y component (i.e. parallel to the ridgeline) combined with a decrease in the U_x component is present especially as we head towards down-ridge. (c.f Fig. 8b, x = 1–1.5, x = 2–2.5 and x = 3–3.5). We can visualize this on Fig. 9a, where we can notice that the computed velocity vectors near the windward surface are tilted towards the U_y component in the WDR direction.

Therefore, we relate the decrease in the ROS in the WUS direction with the increase of α to the flow behaviour discussed above. Furthermore, this increase in the U_y and decrease in the U_x components due to the nature of the slope affects the fire spread in the WDR direction, as we shall see in Section 3.3.

Regarding the LDS direction, the values of $\overline{R'}_{LDS}$ presented in Fig. 10 show that they are relatively low, comparing to the WUS direction with values less than 2.5 NDROS. By looking at the general topology of the adiabatic flow around the hill, which we present by streamlines computed from the simulation in Fig. 11, we can see the formation of two main eddies on the recirculation zone of the hill in the downstream region. These two eddies are driving the flow in directions contrary to the fire spread in the LDS direction. Therefore, the resultant low ROS values are due to the unfavourable combined wind and slope effects.

The instantaneous values of R'_{WUS} and R'_{LDS} in our tests are practically constant for each configuration indicating a quasi-steady behaviour of the fire in both upslope and downslope directions. However, we cannot take further conclusions as the travelled distance by the fire is relatively small to develop a transition behaviour.

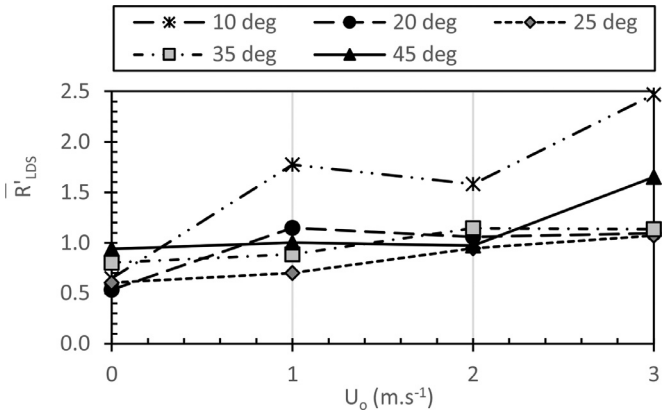

Fig. 10. The average NDROS values on the leeward downslope direction (LDS).

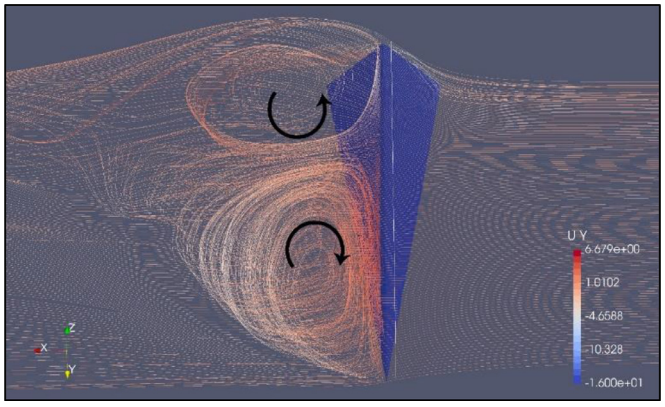

Fig. 11. Overall topology of the flow around the hill for α=45º represented by streamlines, which show the flow separation and the eddies formed in the recirculation zone downstream from the hill. The flow is in the positive x-direction, from right to left and the black arrows show the direction of rotation of the eddies.

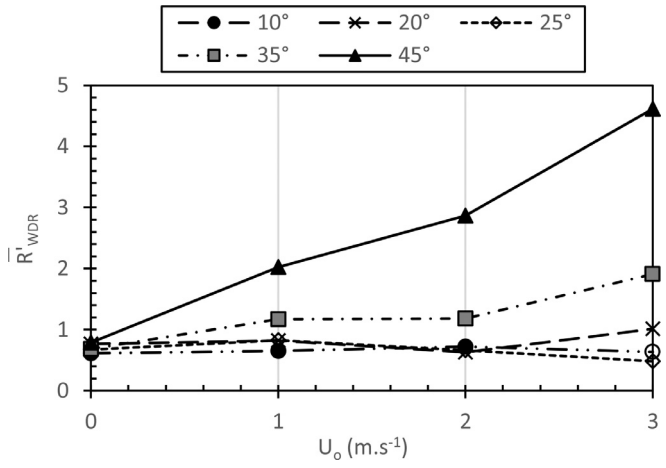

Fig. 12. Average NDROS values on the windward down-ridge direction (WDR) for different values of α and U_o. The not filled point marks are cases where the fire was self-extinguished after advancing a small distance, and the presented value is for that small distance.

3.3. The windward-down-ridge direction (WDR)

For values of α from 10 to 25º, the fire spreads in the WDR direction with $\bar{R}'_{WDR}$ values close to 1 with the fire being self-extinguished in some cases (Fig. 12). For greater values of α, $\bar{R}'_{WDR}$ becomes higher reaching up to 4.5. This fast spread of the fire is also related to the behaviour of the adiabatic flow near the hill's

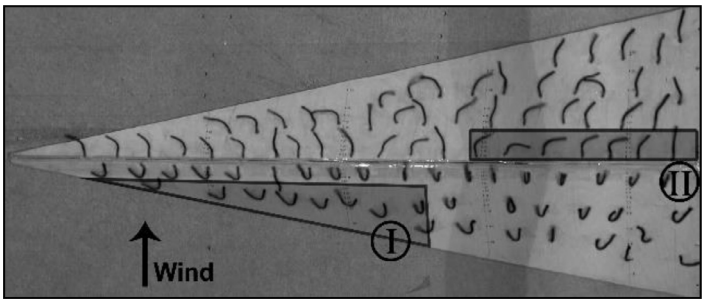

Fig. 13. Flow visualization in adiabatic wind tunnel experiments using wool tufts. The photo is for α=35°

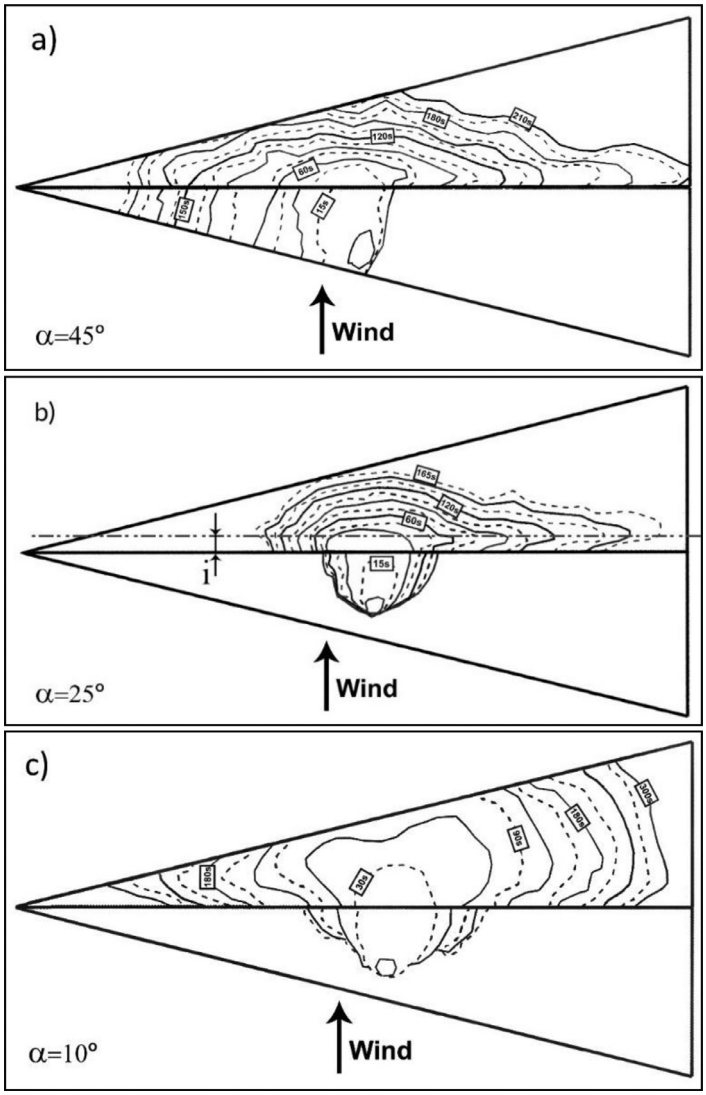

Fig. 14. Fire propagation contour map for different tests. a) for test 3D11.2.45, the time-lapse between frames is 15 s. b) for test 3D3.2.25, the time lap between frames is 15 s, [i] is the distance between the LUR lateral growth and the ridgeline. c) for test 3D32.3.10, the time-lapse between frames is 30 s.

surface. From the flow simulation results in Fig. 8b, we can see that for the lines L3 and L4, there is an increase in the lateral flow (U_y) associated with the increase in α, which can reach up to 25% of the freestream velocity. This behaviour can be visualized in Fig. 9a, where the flow vectors are tilted towards the down-ridge direction. This remark coincides with what we observed during the wind tunnel tests in the absence of fire. On Fig. 13, we can see an image taken of the wool tufts attached to the model where α=35° By observing the tufts in the shaded area (I), we notice that they tend to be orientated more parallel to the ridgeline. The other tested α values (25 and 45°) show similar behaviour where the tufts have similar direction tendency.

Therefore, when α>25º, the flow has a sufficient U_y component to enlarge the fire laterally towards down-ridge to cause the fire to spread with relatively high ROS in the WDR direction as we can see on Fig. 14a. Furthermore, using the laser sheet vi-

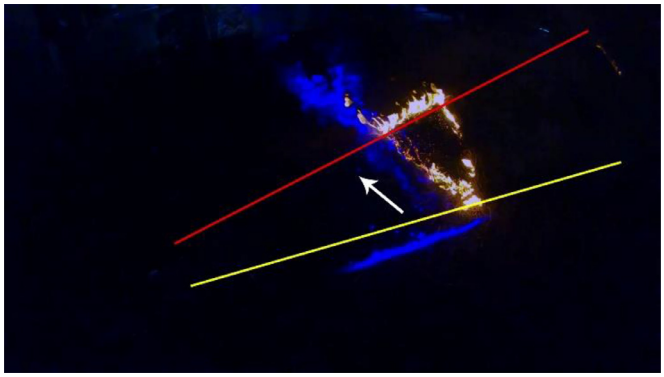

Fig. 15. Snapshot from a video that films the movement of fire generated-smoke that is visualized using a blue laser sheet placed parallel to the windward surface and spaced from it by 10 cm. The image shows the lateral spread of the fire towards WDR and the smoke climbs up-slope with a tilted angle in the direction of the drawn white arrow. The red line represents the ridgeline while the yellow line represents the base of the windward face. The video is filmed for test 3D7.2.35. (For interpretation of the references to colour in this figure legend, the reader is referred to the web version of this article.)

sualization during the fire tests, we observed that the flames of the WDR fire front are fluctuating between tilting towards inside (the burnt area) and outside where they align with the near-surface flow velocity vector seen in the adiabatic flow simulations (Fig 9a). Fig. 15 shows a visualization of the flow using a laser sheet positioned parallel to the windward surface and spaced from it by 10 cm measured perpendicular to the surface. We observed the smoke moving upslope with an inclined angle towards down-ridge. We provide a video as a supplementary material that documents this movement. However, for $\alpha \leq 25^{o}$ values, the fire does not enlarge laterally with high ROS (cf. Fig. 14b).

In Fig. 16, the dynamic behaviour of the fire spread in WDR is analysed for $\alpha = 35^{o}$ and 45^{o}. We can see that the instantaneous values of R'_{WDR} are relatively high in the beginning and then they decrease while the fire moves towards down-ridge. The decrease in the ROS happens as the lateral flow becomes weaker in the lower region since it mixes with the free stream. We consider the behaviour of the fire in the WDR direction as an unexpected behaviour since it spreads in a downslope direction with NDROS values up to 9, and in our tests, we observed a rate of change that can reach up to ~45 NDROS per minute (Table 2).

3.4. The up-ridge directions

Starting with the windward face, the values of $\overline{R'}_{WUR}$ shown in Fig. 17a indicate that the fire spreads relatively slowly in this direction in comparison to the up-ridge direction on the leeward face (LUR). We observed that in all our tests, either the fire has self-extinguished after travelling some distance in the WUR direction or we have $\overline{R'}_{WUR} < 1.4$.

On the LUR direction, there is a strong lateral growth of the fire (fire channelling) as we can see from the average values of $\overline{R'}_{LUR}$ reported in Fig. 17b. For $\alpha = 10^{o}$, we noticed that there is no critical behaviour occurrence as the fire propagates with a typical flanking behaviour ($\overline{R'}_{LUR} \sim 1$) (Fig. 14c). This behaviour is expected as the slope is very small, and the terrain does not modify very much the flow (c.f. Fig. 8 and Annex 1). For values of $\alpha > 10^{o}$, the lateral growth behaviour is evident, where the value of $\overline{R'}_{LUR}$ is between 5 and 6 when $U_o = 3$ m s^{-1}, for the different inclinations. The lateral growth can be seen in the fire contour

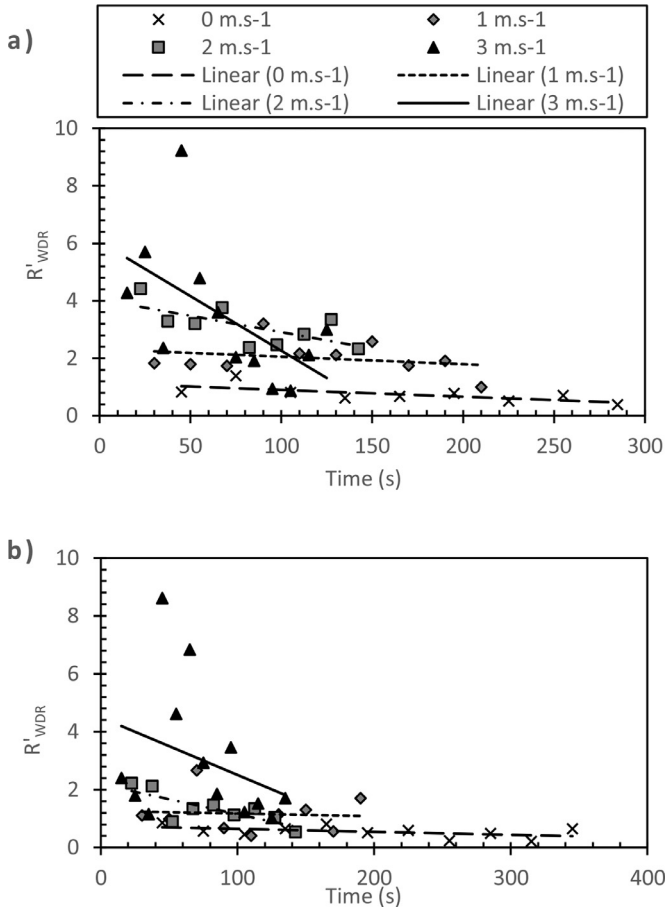

Fig. 16. The instantaneous NDROS values on the windward face in the down-ridge direction (WDR). a) for $\alpha = 45^{\circ}$ b) for $\alpha = 35^{\circ}$ Both for different values of U_o. The legend of (b) is the same as (a).

maps that are shown in Fig. 14a) and b) for tests 3D11.2.45 and 3D3.2.25.

By analysing the variations on the $\overline{R'}_{LUR}$ values in respect to α and U_o with exclusion of the $\alpha = 10^{o}$ case, we notice that the relative variations on NDROS for different α values and a given U_o are small compared to the NDROS variations for different U_o values and a given α (Fig. 17b). We calculated an average rate of increase of 0.48 NDROS per 10^{o} increase in α for a given wind speed, and an average rate of increase of 1.55 NDROS per 1 m.s^{-1} increase in the wind speed (U_o) for a given α value.

The lateral fire spread behaviour in the LUR direction is due to the nature of the local terrain-modified flow on the area, namely a formed eddy in the hill's recirculation zone (cf. Fig. 11). This eddy drives the flow near the ridgeline with a lateral component (negative y-direction) towards up-ridge. The calculated velocity vectors near the surface illustrate the flow direction in the area (Fig. 9b). The result coincides with the flow visualization performed during the wind tunnel tests in the absence of fire, which is noticeable in the shaded area II in Fig. 13. The resultant lateral flow from the eddy near the ridgeline is the main driver for the high ROS lateral spread of the fire in the LUR direction.

Furthermore, during flow visualization tests using the laser sheet, we observed a counter-clockwise circulation movement of the smoke in the upper half of the ridge, which indicates the existence of the predicted eddy in the adiabatic flow simulation

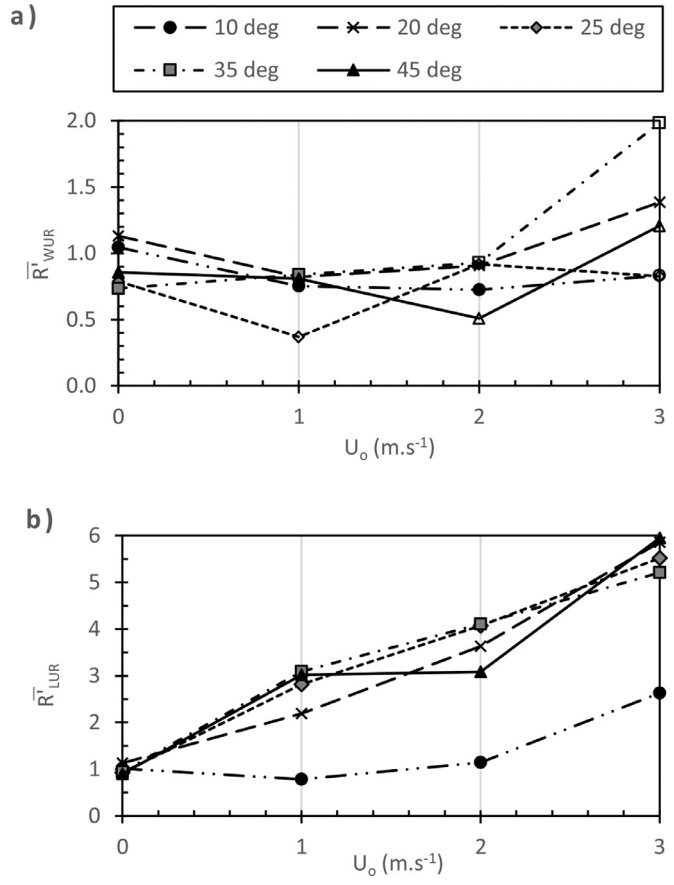

Fig. 17. The average NDROS values. a) On the windward up-ridge direction (WUR). b) On the Leeward up-ridge direction (LUR). Both are for different values of α and U_o. The not filled point marks on (a) are cases where the fire was self-extinguished after spreading for a small distance. The presented values are for that small distance. The legend of (b) is the same as (a).

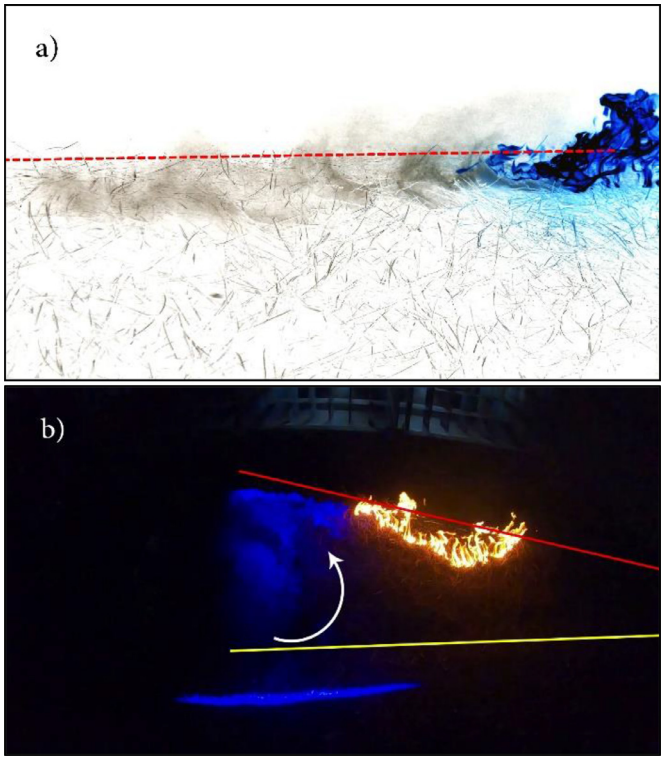

Fig. 18. a) Processed image of the lateral fire growth on the LUR direction showing the movement of a smoke trail (in dark grey) towards the LUR direction. On the image, the fire is in blue, and the red dashed line is the ridgeline — photo from test 3D28.3.20. b) A snapshot from a video that films the movement of fire generated-smoke that is visualized using a blue laser sheet that is placed parallel to the leeward surface and spaced from it by 10 cm. The image shows the lateral spread of fire and the white arrow represents the observed rotational smoke movement. The drawn red line represents the ridgeline while the yellow line represents the base of the leeward face. The video is filmed for test 3D7.2.35. (For interpretation of the references to colour in this figure legend, the reader is referred to the web version of this article.)

(Fig. 11 and Fig. 9b). We also noticed that the generated smoke from the fire forms a trail and moves parallel to the ridgeline towards up-ridge, indicating the flow direction in the region (Fig. 18a). The observed smoke movement consists of a translation motion with a superimposed rotation that appears from time to time. We are providing a video that documents the flow visualization as supplementary material and Fig. 18b shows a snapshot of that video. We must mention also that the LUR direction is an up-slope direction (the ridgeline's slope). However, the angle of the ridgeline relative to the flat surface varies between 2.5º and 10.3º for the α values between 10º and 45º, respectively. Therefore, this slope is not as significant as the slope of the hill's face.

We now look at the dynamic behaviour of the fire spread along LUR direction to understand better the fire channelling process over the sloped-ridgeline hill configuration. The instantaneous values of R'_{LUR} are shown in Fig. 19 for each value of α and U_o as a function of time elapsed since the fire passed the ridgeline. For $\alpha = 10º$ (Fig. 19a), we see that in the presence of wind there is a deceleration of the fire as the NDROS values reduce with time, and they do not exceed 2 in all situations. For higher values of α, where the lateral growth (fire channelling) is present, we see a common acceleration in the fire spread with time, especially for high values of U_o. This acceleration happens with a rate of change that can reach up to ~19 NDROS per minute. In our tests, we observed that the instantaneous value of NDROS could reach up to 9 for some time steps.

To interpret this fire spread acceleration in the LUR direction, we used values of the flow velocity from the adiabatic flow simulation along a line parallel to the ridgeline spaced from it by 0.015 m, and 0.01 m above the surface (see the dashed line in Fig. 14b). We used a non-dimensional coordinate ζ in this analysis that indicates the relative distance along the measuring parallel line, where it is equal to 0 at the top of the hill (up-ridge) and 1 near the base (down-ridge). In Fig. 20a we can notice that U/U_o has a minimum value near $\zeta \approx 0.25$ and increases to the right and left of that point to reach maximum value of around 0.45. By looking to U_y in Fig. 20b, we can find that U_y/U_o values have similar behaviour where U_y is zero at $\zeta \approx 0.25$ and increases towards right and left from that point as well, but with differences in the flow direction (i.e. negative in up-ridge and poitive in down-ridge). The change of the velocity modulus along this line is consistent with the change of U_y, which means that the modulus of U is governed mainly by the y-component. This can be visulaized by the velocity vectors plotted near the ridgeline in Fig. 9b.

In Fig. 21, we plotted the change in the computed y-component of the adbatic flow velocity together with the R'_{LUR} and R'_{LDR} along the same line as before in Fig. 20. We can notice that the trend of change in the rate of spread of the fire is similar to the trend of change in the U_y. Therefore, we relate the fire spread acceleration in the LUR to the behaviour of the terrain-modified flow in the area.

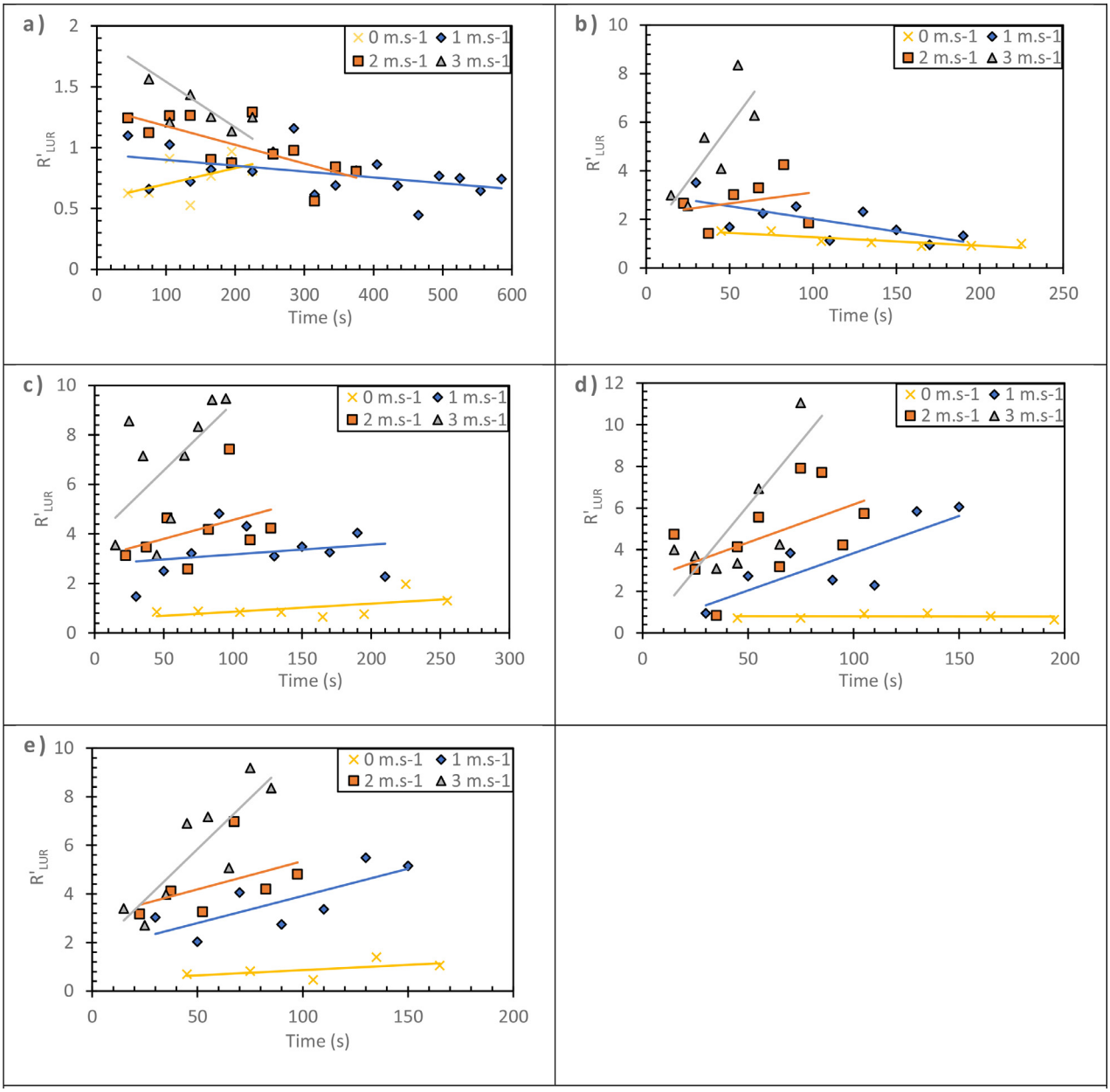

Fig. 19. Instantaneous NDROS values on the Leeward up-ridge direction for each inclination with different wind velocities. a) 10° b) 20° c) 25° d) 35° e) 45°

3.5. The leeward-down-ridge direction (LDR)

In the LDR direction, the fire enlarged as well but not as rapidly as it does in the opposite direction, LUR. In fact, for $\alpha \leq 25º$ the fire propagates with $\bar{R}'_{LDR} < 2$. Nevertheless, in our tests with $\alpha = 35º$ and 45º, the fire advanced in the LDR direction with relatively greater ROS comparing to the lower values of α (Fig. 22). We relate the high ROS on these two cases to long flames that were generated from the burning fire front on the other side of the hill (windward) and trough the fuel on the leeward side, which is a result of the strong down-ridge lateral flow discussed previously. The flames ignite the fuel over the leeward face after the ridgeline. This effect is due to the relatively small size of the model. This conclusion is reached since we observed that these long flames drag the fire front in the LDR direction over both faces. Also, we can see on the contour map in Fig. 14c that the two fronts over the windward and leeward faces are advancing together towards down-ridge. However, we cannot ignore that the adiabatic flow in the area has relatively high U_y values as observed on the flow study (Fig. 9b and Fig. 20) which could be contributing to the fire spread on the LDR direction as well. We would require a larger model to investigate this problem more carefully, which is not possible at present due to the limitation of the wind tunnel's working section size.

4. Conclusion

The experiments and flow simulations discussed above show that the fire spread over a sloped-ridgeline hill configuration for various wind conditions is very complex. The terrain-modified flow enhanced by the fire-induced convection results in a locally accelerated flow that drives the fire laterally over the sloped-ridgeline hill configuration. Two possibly unusual or unexpected lateral fire spreads occur: one in a down-ridge direction over the windward face and the other in an up-ridge direction over the leeward face. We consider these lateral spreads as unexpected fire behaviour as the fire spreads with a high rate of spread in a direction other

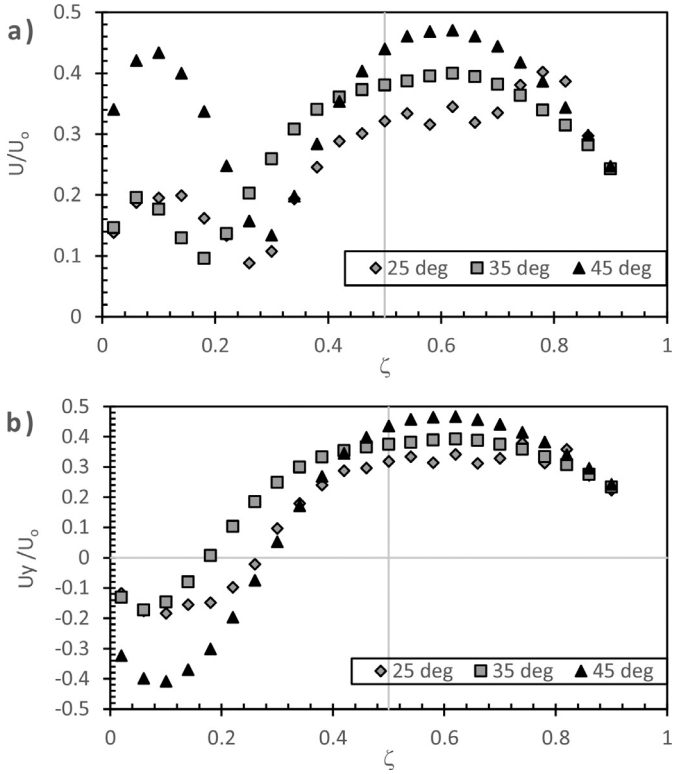

Fig. 20. Flow velocity results from the CFD simulation obtained at points along a line parallel to the ridgeline and spaced from it by 0.015 m and over the leeward surface by 0.01 m. a) Velocity component in the y-direction (U_y). b) Velocity modulus. The velocity is presented dimensionless where the values are divided by the inlet stream velocity (U_o=8 m.s^{-1}). The non-dimensional coordinate ζ corresponds to the relative distance of the point along the measuring line, where zero corresponds to the tip point at up-ridge, and 1 is at down-ridge.

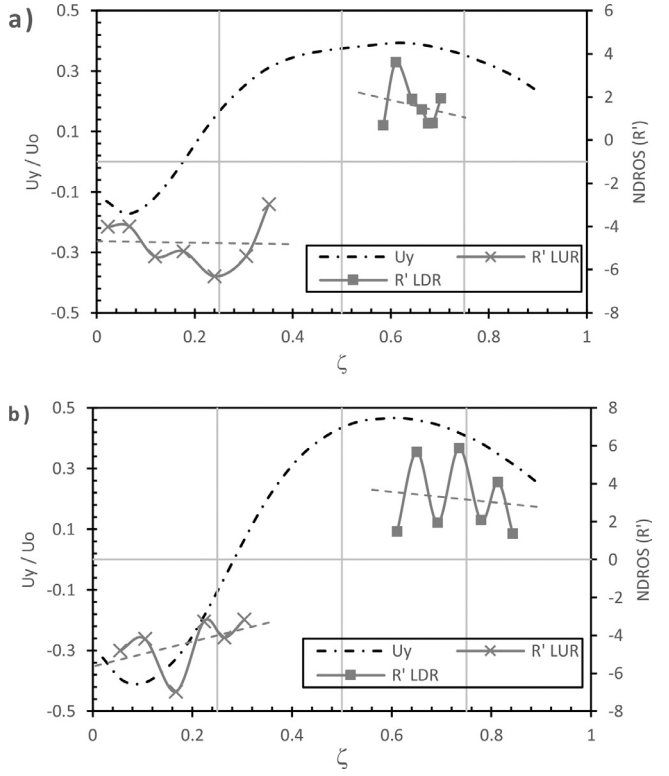

Fig. 21. Results of the flow velocity component in the y-direction (U_y) obtained from the CFD simulation along a parallel line to the ridgeline and spaced from it by 0.015 m and over the leeward surface by 0.01 m similar to Fig. 20, together with the non-dimensional rate of spread of the fire (NDROS) in the LDR and LUR directions. a) for α=45° b) for α=35° The velocity is presented dimensionless where the values are divided by the inlet stream velocity (U_o=8 m.s^{-1}). The non-dimensional coordinate ζ corresponds to the relative distance of the point along the measuring line, where zero corresponds to tip point at up-ridge, and 1 is at down-ridge. The positive and negative values in the y-axis correspond to the direction of the flow or fire spread, where the positive is down-ridge direction and vice versa.

than the main wind stream direction, even if the down-ridge lateral spread over the windward face is, in fact, a downslope direction.

This study highlights also the importance of the terrain-modified flow mechanisms over complex terrains where they can generate critical fire behaviour in some unexpected directions, in which they can put the firefighting teams in a dangerous situation if they are not aware of this potential fire behaviour.

The authors intend to extend this experimental and numerical program considering other wind directions and hill configurations and scales.

Declaration of Competing Interest

The authors declare that they have no known competing financial interests or personal relationships that could have appeared to influence the work reported in this paper.

Acknowledgements

The authors are grateful to Professor Almerindo Domingues Ferreira, from DEMUC, for his support to perform the wind tunnel tests, to Nuno Luis and António Cardoso for their help to carry on the fire investigation tests. Also, the authors acknowledge the assistance of the team of the Laboratory of Simulation in Energy and Fluids (LASEF) from IST/IDMEC, namely Professor José Carlos Pereira and Duarte Albuquerque, for allocating resources to perform the numerical simulations.

Funding: This work was supported by the Portuguese Foundation for Science and Technology through the projects "IM-FIRE - Intelligent Management of Wildfires" (PCIF/SSI/0151/2018) and "FIRESTORM - Weather and Behaviour of Fire Storms" (PCIF/GFC/0109/2017).

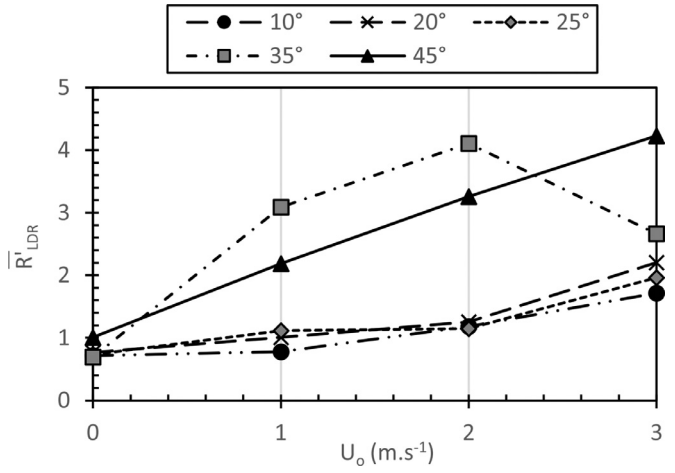

Fig. 22. Average NDROS values on the leeward down-ridge direction for different values of α and U_o.

Annex 1

Fig. A1, Fig. A2.

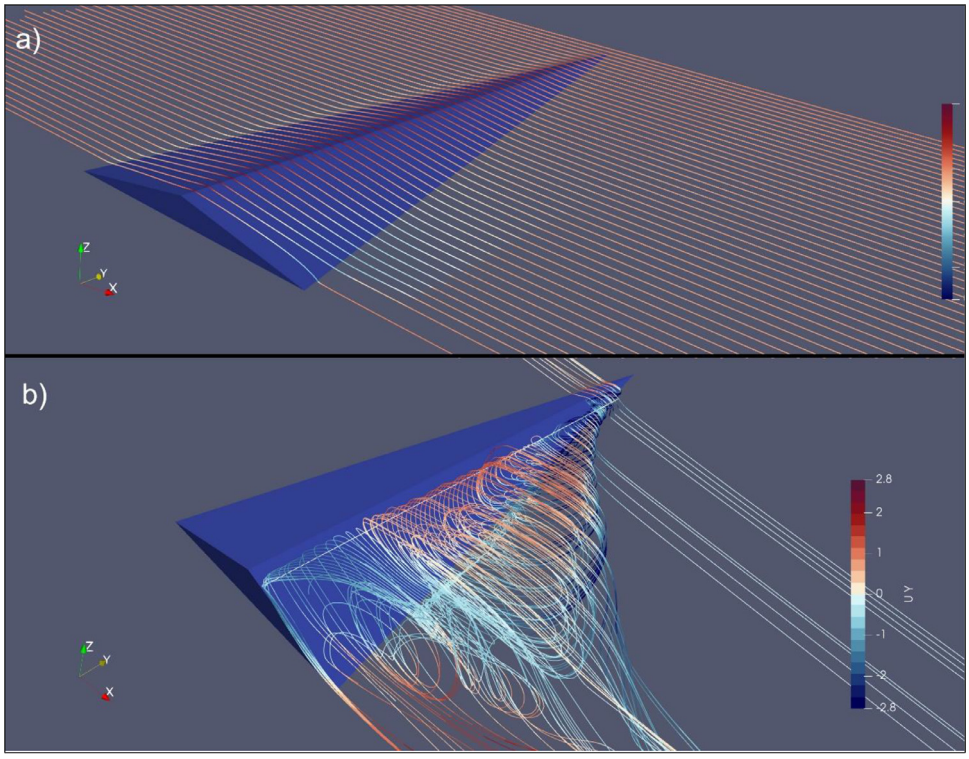

Fig. A1. Overall topology of the simulated adiabatic flow around the hill represented by streamlines. The flow is in the positive x-direction. a) for α=10° b) for α=20° The streamlines are sourced from the same line for both (a) and (b) near the ridgeline over the leeward side.

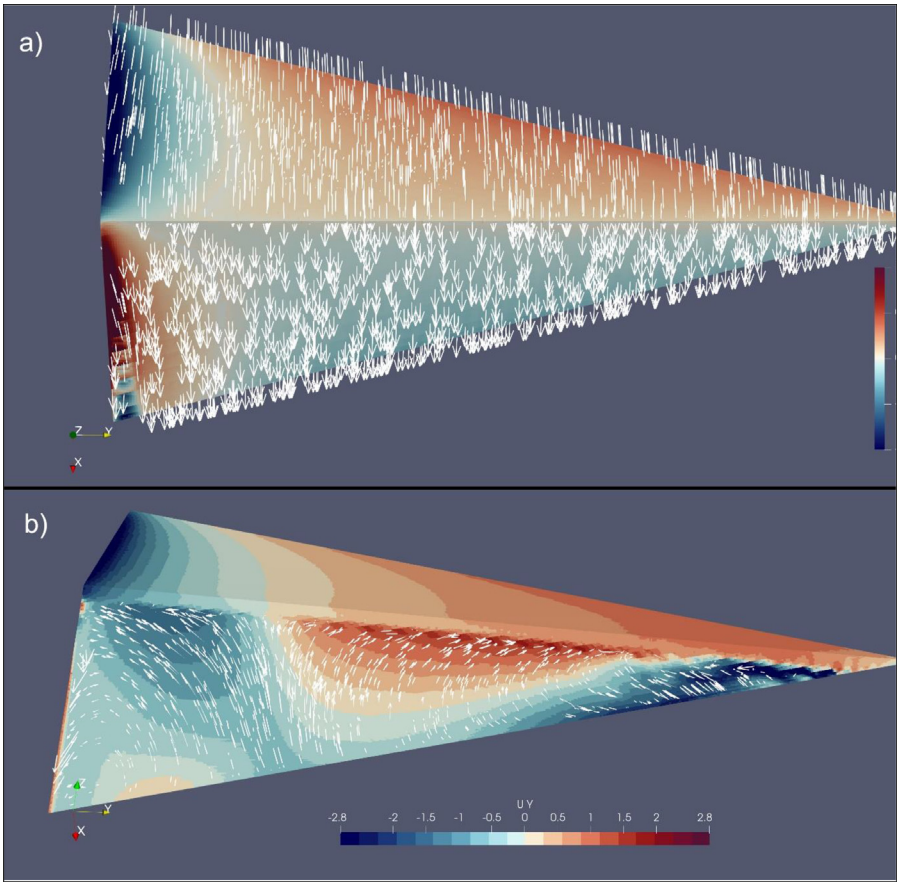

Fig. A2. Numerical results for the field of the velocity component in the y-direction (U_y) on a parallel plane to the hill's leeward face and spaced from it by 0.01 m along with the velocity vectors. a) for α=10° b) for α=20°

References

[1] A.G. McArthur, A. Forestry, T. Bureau, A.G. McArthur, Fire behaviour in eucalypt forests, Canberra (1967).

[2] R.M. Nelson, An effective wind speed for models of fire spread, Int. J. Wildl. Fire. 11 (2002) 153–161, doi:10.1071/WF02031.

[3] D.X. Viegas, Slope and wind effects on fire propagation, Int. J. Wildl. Fire. 13 (2004) 143–156, doi:10.1071/WF03046.

[4] R.A. Linn, J.A. Winterkamp, C.B. Edminster, J.J. Colman, W.S. Smith, Coupled influences of topography and wind on wildland fire behaviour, Int. J. Wildl. Fire. 16 (2007) 183–195, doi:10.1071/WF06078.

[5] A.L. Sullivan, Wildland surface fire spread modelling, 1990–2007. 1: physical and quasi-physical models, Int. J. Wildl. Fire. 18 (2009) 349–368, doi:10.1071/WF06144.

[6] A.L. Sullivan, Wildland surface fire spread modelling, 1990–2007. 2: empirical and quasi-empirical models, Int. J. Wildl. Fire. 18 (2009) 369, doi:10.1071/wf06142.

[7] A.L. Sullivan, Wildland surface fire spread modelling, 1990-2007. 3: simulation and mathematical analogue models, Int. J. Wildl. Fire. 18 (2009) 387, doi:10.1071/wf06144.

[8] N. Liu, J. Wu, H. Chen, X. Xie, L. Zhang, B. Yao, J. Zhu, Y. Shan, Effect of slope on spread of a linear flame front over a pine needle fuel bed: experiments and modelling, Int. J. Wildl. Fire. 23 (2014) 1087–1096, doi:10.1071/WF12189.

[9] J.J. Sharples, R.H.D. McRae, S.R. Wilkes, Wind-terrain effects on the propagation of wildfires in rugged terrain: fire channelling, Int. J. Wildl. Fire. 21 (2012) 282–296, doi:10.1071/WF10055.

[10] C.C. Simpson, J.J. Sharples, J.P. Evans, M.F. McCabe, Large eddy simulation of atypical wildland fire spread on leeward slopes, Int. J. Wildl. Fire. 22 (2013) 599–614, doi:10.1071/WF12072.

[11] J.R. Raposo, S. Cabiddu, D.X. Viegas, M. Salis, J. Sharples, Experimental analysis of fire spread across a two-dimensional ridge under wind conditions, Int. J. Wildl. Fire. 24 (2015) 1008–1022, doi:10.1071/WF14150.

[12] C.C. Simpson, J.J. Sharples, J.P. Evans, Resolving vorticity-driven lateral fire spread using the WRF-Fire coupled atmosphere-fire numerical model, Nat. Hazards Earth Syst. Sci. 14 (2014) 2359–2371, doi:10.5194/nhess-14-2359-2014.

[13] J.-.L. Dupuy A, J.Maréchal B, D. Portier, J.-.C. Valette, The effects of slope and fuel bed width on laboratory fire behaviour, Int. J. Wildl. Fire. 20 (2011) 272–288, doi:10.1071/WF09075.

[14] C.G. Rossa, D.A. Davim, D.X. Viegas, Behaviour of slope and wind backing fires, Int. J. Wildl. Fire. 24 (2015) 1085–1097, doi:10.1071/WF14215.

[15] R.H.D. McRae, Breath of the dragon – observations of the January 2003 ACT Bushfires, Proc. 2004 Australas. Bushfire Res. Conf. May 2004, Adelaide. (2004).

[16] D.X. Viegas, A. Simeoni, Eruptive behaviour of forest fires, Fire Technol 47 (2011) 303–320, doi:10.1007/s10694-010-0193-6.

[17] D.X. Viegas, A. Rodrigues, A. Abouali, M. Almeida, J. Raposo, Fire downwind a flat surface entering a canyon by lateral spread, Fire Saf. J. 122 (2021) 103349, doi:10.1016/j.firesaf.2021.103349.

[18] H.G. Weller, G. Tabor, H. Jasak, C. Fureby, A tensorial approach to computational continuum mechanics using object-oriented techniques, Comput. Phys. 12 (1998) 620, doi:10.1063/1.168744.

[19] C. Greenshields, SnappyHexMesh, OpenFOAM v4 User Guid. (2015). https://cfd.direct/openfoam/user-guide/v4-snappyHexMesh/ (accessed February 21, 2018).

[20] F.R. Menter, M. Kuntz, R. Langtry, Ten years of industrial experience with the SST turbulence model, Turbul. Heat Mass Transf. 4 4 (2003) 625–632, doi:10.4028/www.scientific.net/AMR.576.60.

[21] A. Abouali, D.X. Viegas, Fire ROS calculator: a tool to measure the rate of spread of a propagating wildfire in a laboratory setting, J. Open Res. Softw. 7 (2019), doi:10.5334/jors.221.

[22] D.X. Viegas, Parametric study of an eruptive fire behaviour model, Int. J. Wildl. Fire. 15 (2006) 169–177, doi:10.1071/WF05050.

[23] D.X. Viegas, L.P.C. Neto, Wall shear-stress as a parameter to correlate the rate of spread of a wind induced forest fire, Int. J. Wildl. Fire. 1 (1991) 177–188, doi:10.1071/WF9910177.